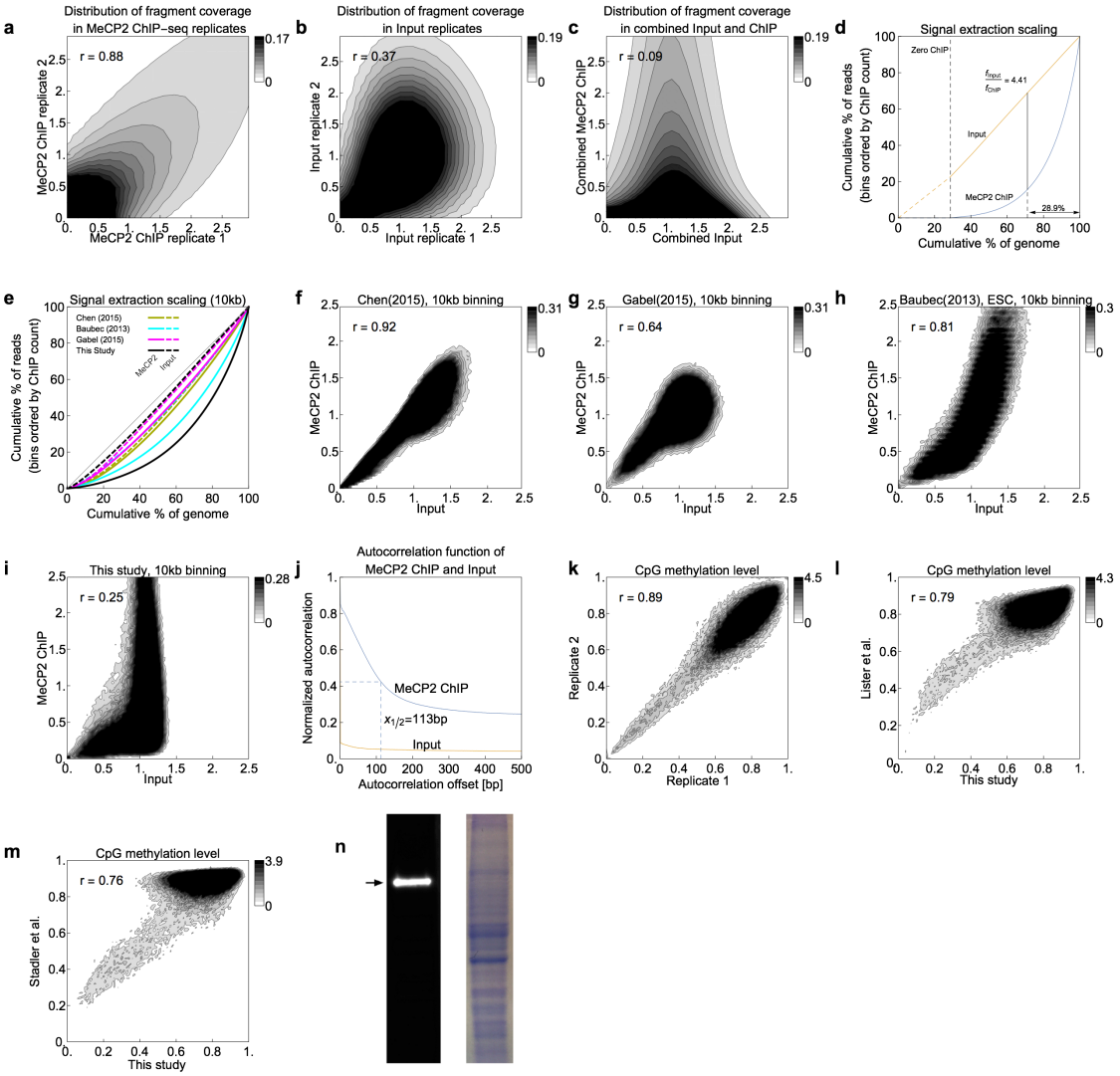

SUPPLEMENTARY FIGURE 1: Comparisons of the biological replicates of ChIP-seq, Input and Bisulfite-seq. (**a**) Density plot of MeCP2 ChIP-seq genome coverage (calculated using tiled 150 bp windows) shows high correlation between the replicates. (**b**) Density plot of Input in replicates. (**c**) Density plot of combined MeCP2-ChIP vs. combined Input shows no correlation. (**d**) Signal extraction scaling plot used for inferring the relative normalization of the ChIP and Input tracks. The pairs of read coverage in ChIP and Input (n_{ChIP}, n_{Input}) are calculated across the genome, and this list of pairs is ordered by n_{ChIP}. The curves indicate cumulative fraction (y-axis) of n_{ChIP}- (blue) and n_{Input}-reads (yellow) as a function of rank in the list (x-axis). The black vertical line shows the point of maximal difference between MeCP2 ChIP and Input and indicates the fraction of genome enriched by the ChIP. (**e**) Signal extraction scaling analysis of published MeCP2 ChIP-seq data sets using 10 kb windows[1-3]. (**f-i**) Density plot of MeCP2 ChIP vs. Input for the published data sets and for this study using 10kb binning. The X chromosome was filtered out since male mice only have one copy (and thus half the coverage). (**j**) Autocorrelation function of MeCP2 ChIP and Input using strand-specific counts of mapped reads at single base pair resolution. The correlation functions have been normalized for sequencing depth as described in the Supplementary Methods section. (**k**) Distribution plot of the methylation levels in the two biological replicates using 10 kb binning. (**l**) Same as **k** but comparing this study to Lister et al.[4]. (**m**) Same as **k** but comparing this study to Stadler et al.[5]. (**n**) Full-length Western blot showing the antibody specificity. Main olfactory epithelium (MOE) was harvested from two adult C57BL/6J mice. Cell lysate was obtained by homogenization in 300 µl of Tris Buffered Saline pH7.2 with proteinase inhibitors (Roche, #11836153001) followed by addition of 4X SDS PAGE loading dye. Aliquots (10 µl) of MOE extract were loaded on 10% SDS PAGE and stained with Coomassie blue, shown on the right; an equal amount of the extract was used for western blotting using 1.2 ng μl^{-1} of MeCP2 antibody (Diagenode, pAb-052-050), shown in the left. Arrow indicates positive band for MeCP2 binding.

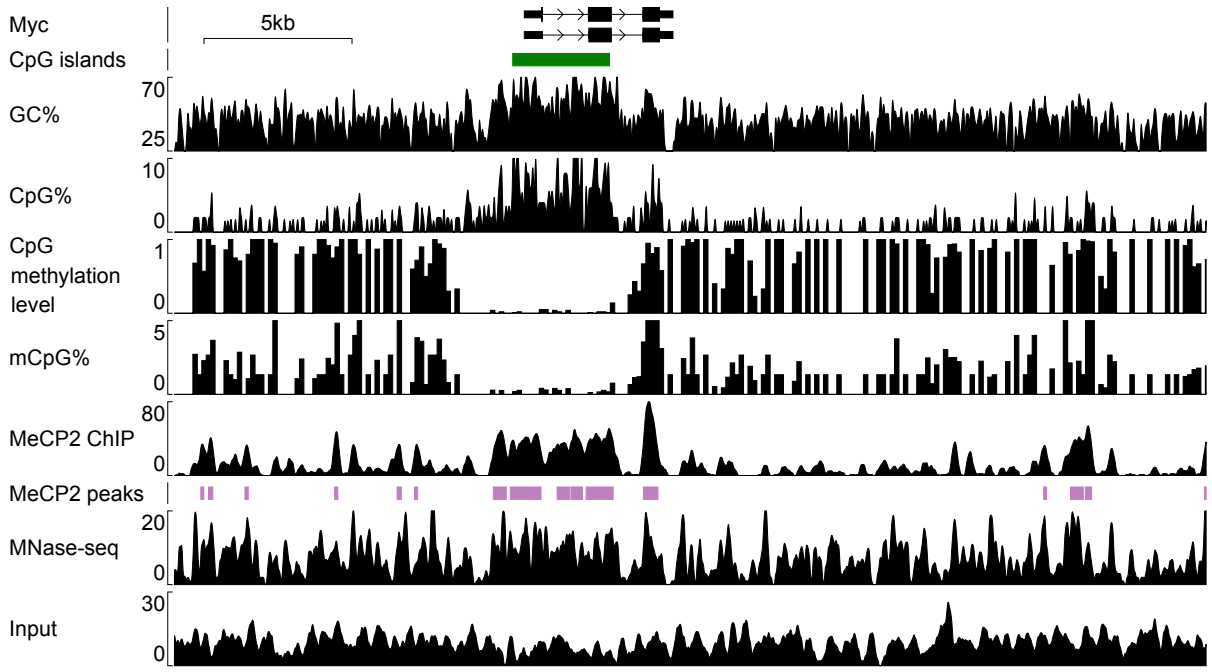

SUPPLEMENTARY FIGURE 2: Sequence GC content, CpG methylation, MNase-seq coverage and ChIP-seq coverage in the region surrounding *Myc*.

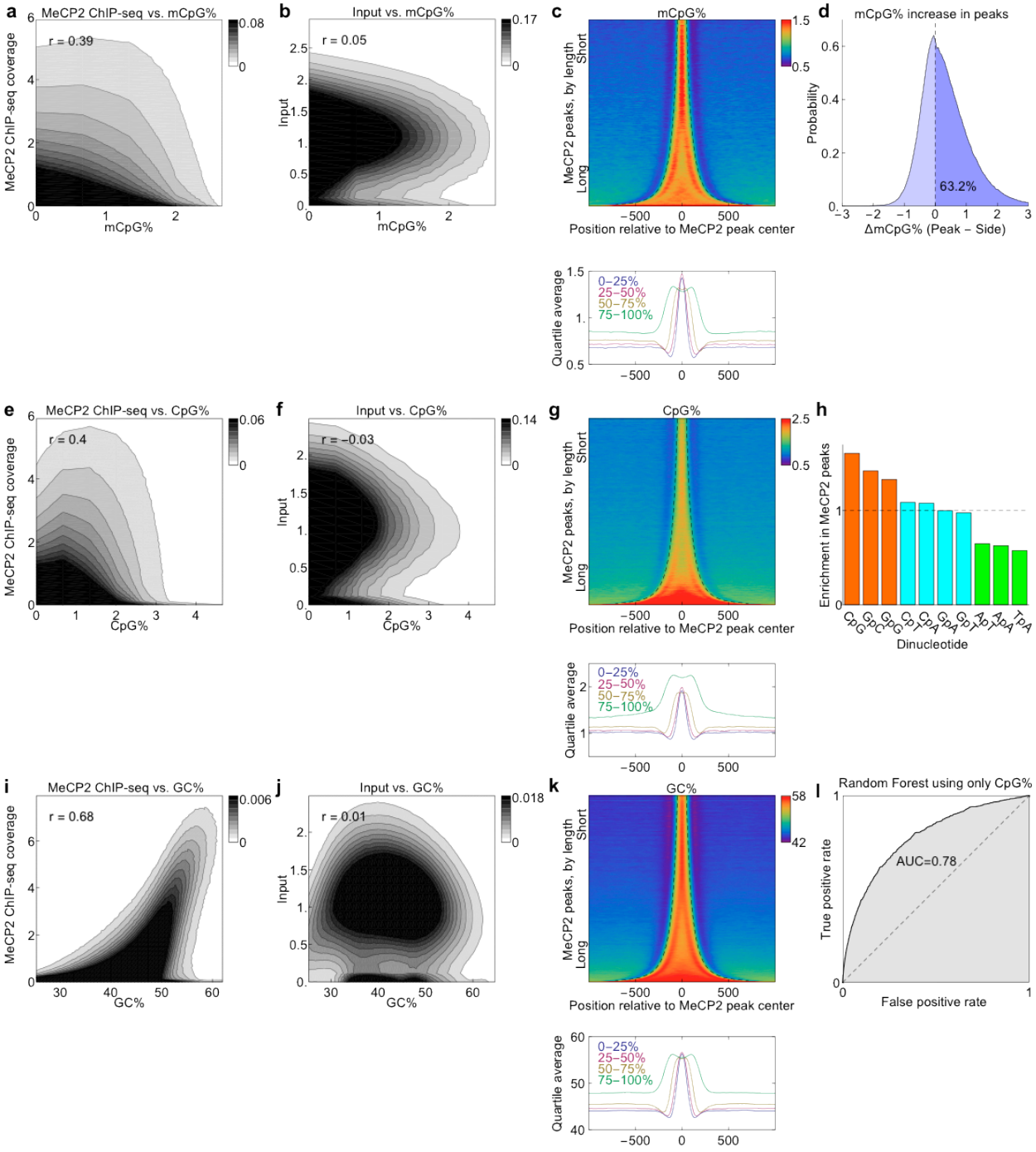

SUPPLEMENTARY FIGURE 3: Sequence and methylation content versus ChIP-seq and Input fragment coverage. (**a**) Distribution plot showing the probability density (shade) of mCpG% vs. MeCP2 ChIP-seq fragment coverage. (**b**) Same as **a** but showing mCpG% vs. Input. (**c**) mCpG% (color) in regions surrounding MeCP2 peaks (dashed lines). The bottom plot shows the median CpG% in peaks organized into peak width quartiles. (**d**) Distribution of the difference in mCpG% between peaks and the adjacent regions. (**e**) Same as **a** but showing CpG% vs. MeCP2 ChIP-seq. (**f**) Same as **a** but showing CpG% vs. Input. (**g**) CpG% (color) in regions surrounding MeCP2 peaks. (**h**) Dinucleotide enrichment in MeCP2 peaks relative to peaks shifted randomly by ±5 kb. The dashed line indicates no enrichment. (**i**) Same as **a** but showing GC% vs. MeCP2 ChIP-seq. (**j**) Same as **a** but showing GC% vs. Input. (**k**) GC% (color) in regions surrounding MeCP2 peaks. (**l**) ROC-curve for predicting MeCP2 ChIP-seq peaks using Random Forest regressor based on CpG% in 200 bp windows. Plots **a-c**, **e-g** and **i-k** use 150 bp windows.

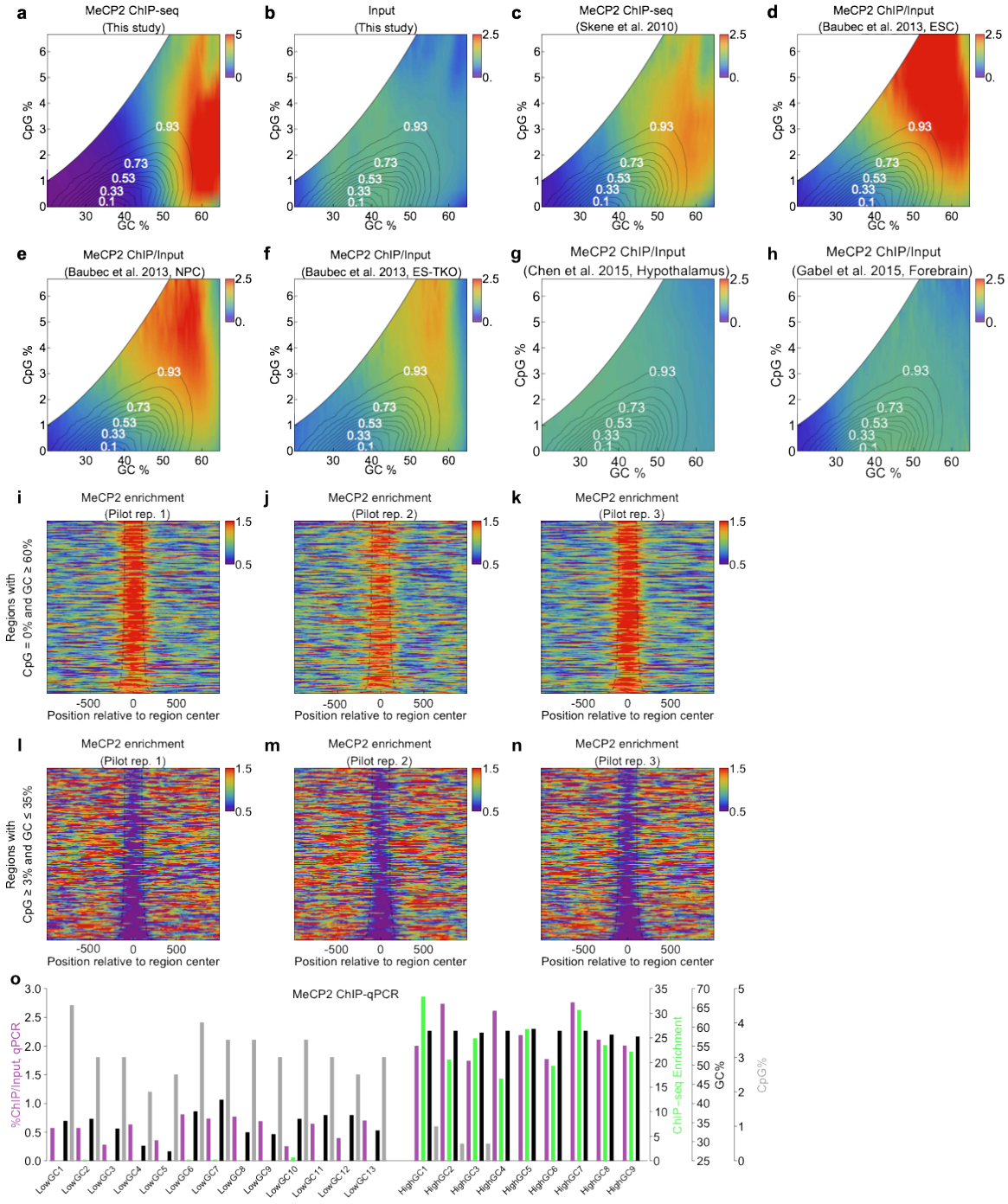

SUPPLEMENTARY FIGURE 4: GC%- and CpG%-dependence of (**a**) MeCP2 ChIP-seq, (**b**) Input, (**c**) MeCP2 ChIP-seq from Skene et al. 2010, (**d**) MeCP2/Input in ES cells from Baubec et al.[1], (**e**) MeCP2/Input in ES cell-derived neuronal progenitor cells (NPC) from Baubec et al.[1], (**f**) MeCP2/Input in Dnmt1, Dnmt3a, and Dnmt3b triple knockout (TKO) ES cells from Baubec et al.[1], (**g**) MeCP2/Input in hypothalamus from Chen et al.[3], (**h**) MeCP2/Input in forebrain from Gabel et al.[2]. MeCP2 enrichment was normalized by sequencing depth in **d**-**h**. (**i-n**) Same as Fig. 2a,e but using three pilot MeCP2 ChIP-seq data sets. (**o**) ChIP-qPCR validation (purple) of MeCP2 ChIP-seq profile (green) in regions with either high GC% and low CpG% or low GC% and high CpG%. Three technical replicate measurements were performed on each of three biological replicate samples. The primer coordinates and sequences are given in Supplementary Table 2. 200 bp windows centered at the qPCR regions were used for calculating GC% and CpG%.

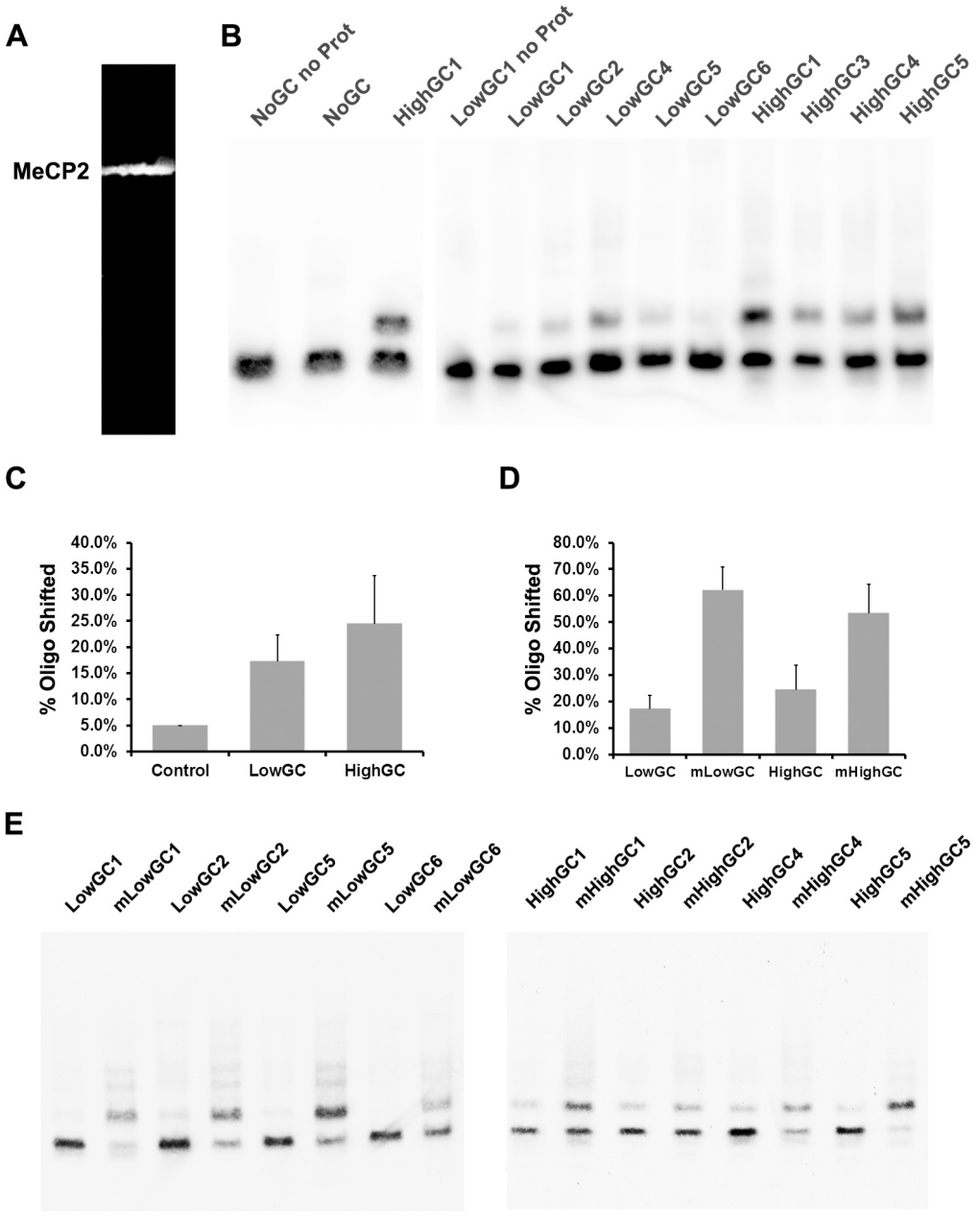

SUPPLEMENTARY FIGURE 5: MeCP2 binding affinity evaluated by EMSA. (**a**) Recombinant MeCP2 isoform2 purified from bacterial lysate via FPLC and confirmed by western blotting. (**b**) Equal amounts of MeCP2 were used to evaluate binding to double-stranded unmethylated oligos containing different GC% (see Supplement Table 3 for oligo information; representative MeCP2-oligo bindings are shown). All EMSA reactions contains poly-dA:dT as competitor DNA (see supplemental methods for detail). Serving as control, first two lanes show an oligo with no GC (Biotin-attattattattattattattattattattattattattattattattattat) in the binding reaction without and with the presence of MeCP2 protein, respectively. In addition, the fourth lane also without the presence of MeCP2 serves as a control to indicate the location of unbound oligos. (**c**) Densitometry analysis of the EMSA blots. With 6 lowGC and 8 highGC oligos tested, higher affinity of MeCP2 towards highGC oligos was observed (mean±SD: 17.3±5.0% vs. 24.5±9.2%; one-sided t-test p-value = 0.04; 4 rounds of EMSA blots were performed for each oligo). (**d**) MeCP2 binds methylated oligos with higher affinity. Each methylated oligo contains the same sequence as the non-methylated version and has one symmetrically methylated CpG on both strands. 2 rounds of EMSA blots were performed for each oligo. Error bars in **c** and **d** indicate standard deviation. (**e**) Representative MeCP2-DNA interactions are shown, comparing side-by-side the MeCP2 binding to methylated and unmethylated oligos.

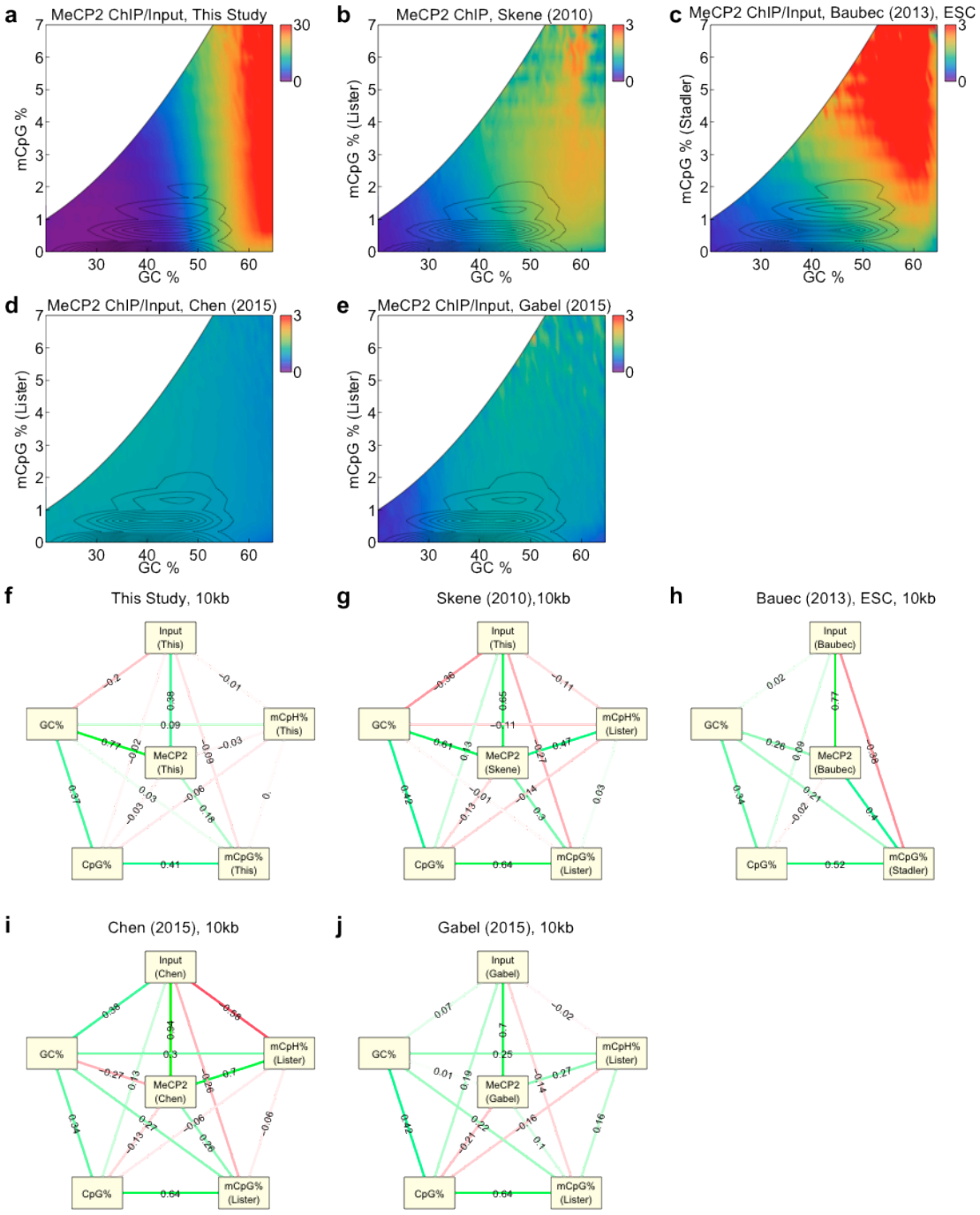

SUPPLEMENTARY FIGURE 6: Methylation- and sequence-dependence of MeCP2 ChIP enrichment. (**a**) GC%- and mCpG%-dependence of the mean MeCP2 enrichment (colors) calculated using 150 bp windows and signal extraction scaling. (**b**) Same as **a** but using MeCP2 ChIP-seq data from Skene et al.[6] (no Input was available) and methylation data from Lister et al.[4]. (**c**) Same as **a** but using ESC MeCP2 ChIP-seq and Input data from Baubec et al.[1] and methylation data from Stadler et al.[5]. (**d**) Same as **a** but using MeCP2 ChIP-seq and Input data from Chen et al.[3] and methylation data from Lister et al.[4]. (**e**) Same as **a** but using forebrain MeCP2 ChIP-seq and Input data from Gabel et al.[2] and methylation data from Lister et al.[4]. MeCP2 enrichment was normalized by sequencing depth in **c**-**e**. (**f-j**) Gaussian graphical models describing the full partial correlations between the MeCP2 ChIP, Input, GC%, CpG%, mCpG% and mCpH% at 10 kb resolution, see Fig. 3b-f and Methods.

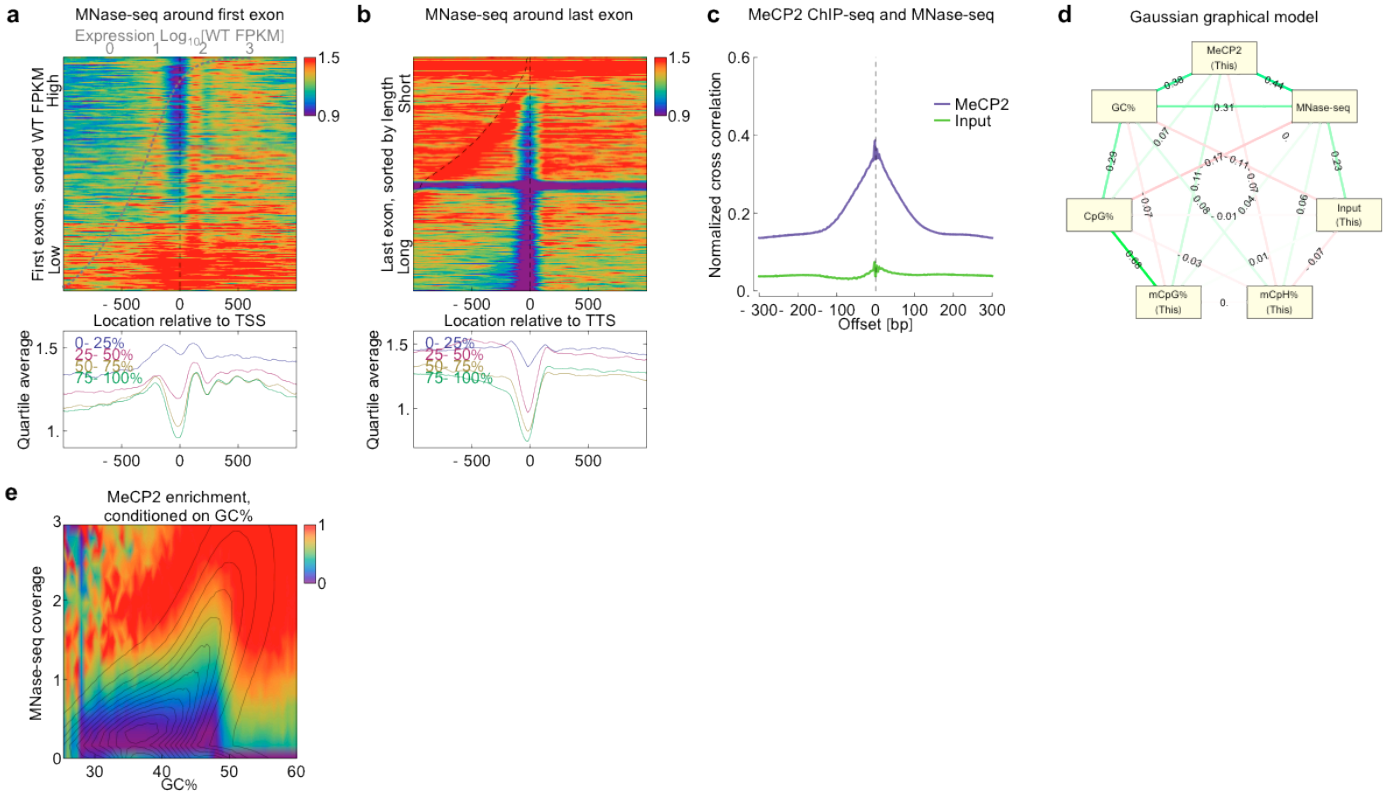

SUPPLEMENTARY FIGURE 7: Structure of the MNase-seq profile. (**a**-**b**) Alignment plots for WT MNase-seq read densities (color) around TSS and TTS. The dashed vertical lines indicate TSS and TTS, respectively. The TSSs are sorted by expression, as indicated by curved gray dashed line. The TTSs are sorted by length of the last exon, and the dashed black curves indicate the outlines of the exons. (**c**) Normalized cross-correlation between MeCP2 (ChIP and Input) and MNase-seq. The correlation coefficients have been normalized for sequencing depth (see Supplementary Methods). (**d**) Gaussian graphical model after including the MNase-seq coverage, see Fig. 3b. (**e**) Dependence of MeCP2 enrichment on nucleosome occupancy. At each value of GC%, the MeCP2 enrichment was linearly transformed to span [0,1] in order to show the conditional dependence of MeCP2 on nucleosome occupancy (color). The contours indicate the genome-wide joint distribution *p*(GC%,MNase-seq).

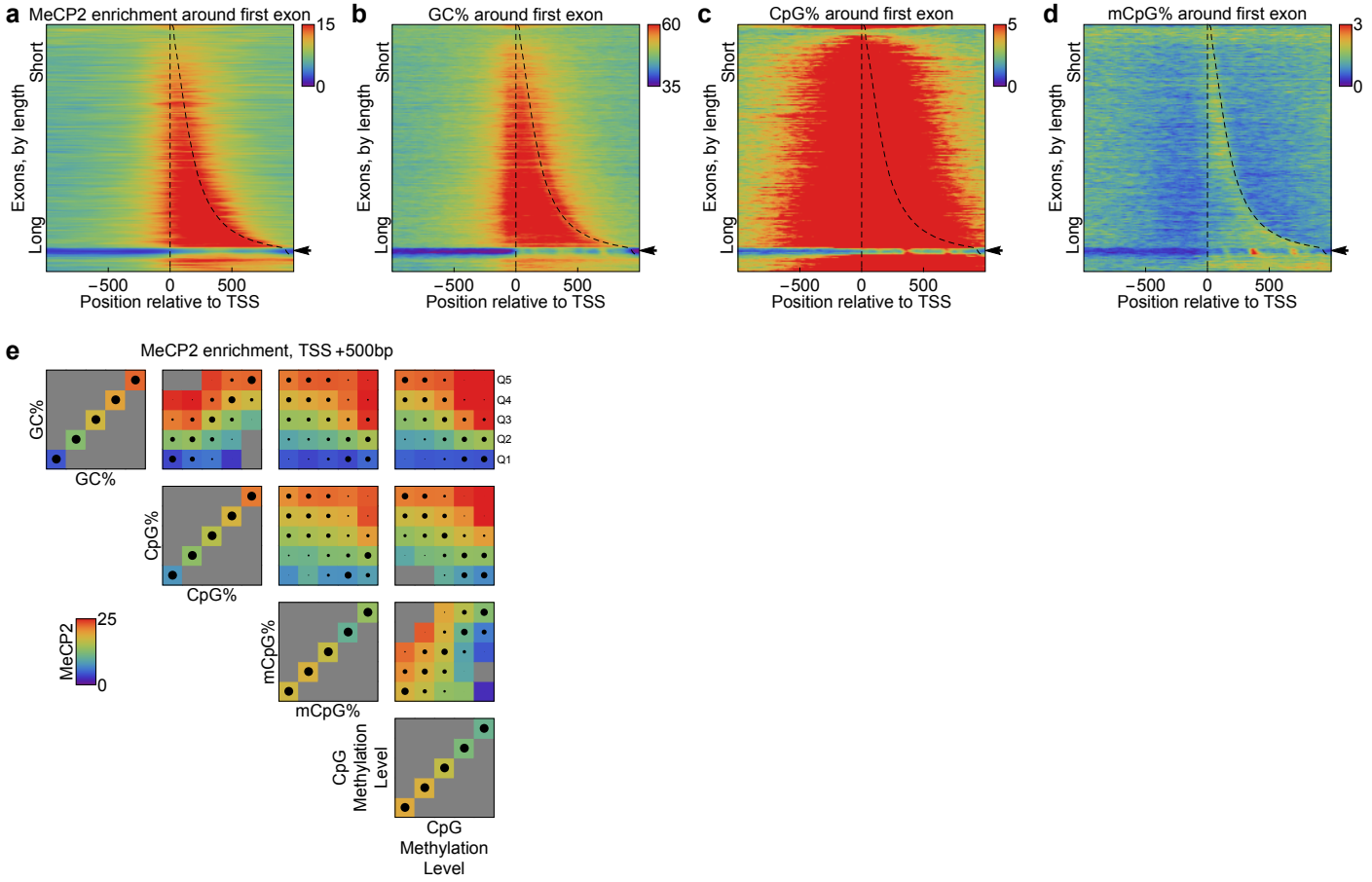

SUPPLEMENTARY FIGURE 8: MeCP2 binding and sequence content around TSSs. (**a**) Alignment plots showing MeCP2/Input-enrichment (color) around TTSs. (**b**) Same as **a** but showing aligned GC%. (**c**) Same as **a** but showing aligned CpG%. (**d**) Same as **a** but showing aligned mCpG%. A cluster of genes (arrows) displays low MeCP2 binding, GC% and CpG%. These genes have length in the range 930 bp to 950 bp and 79% of them are Olfr gene family members, which are known to have low GC%[7]. (**e**) GC%, CpG%, mCpG% and CpG methylation level dependence of the MeCP2 enrichment 500 bp downstream of TSSs. Each subplot shows how the mean MeCP2 enrichment (color) depends on a pair of covariates after grouping by quintile (columns and rows in subplots). Gray indicates quintile combinations without data. The areas of the black disks show the conditional probability of a column in a subplot given a row (or vice versa). The direction of the color gradient indicates the strongest dependence of the MeCP2 enrichment. Bands of large disks indicate variables that co-vary; e.g. GC% and mCpG% anti-correlate.

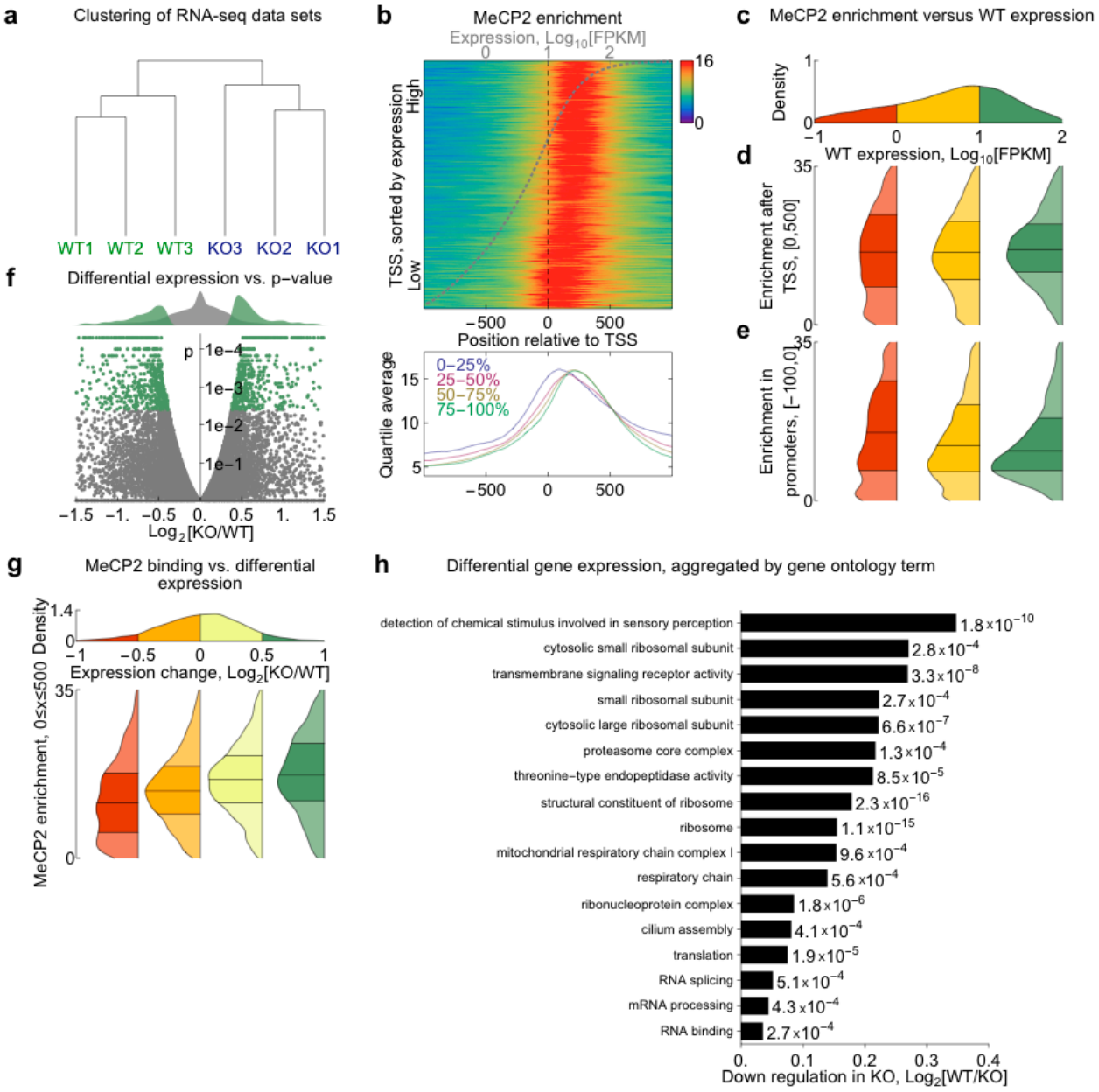

SUPPLEMENTARY FIGURE 9: Relationship between MeCP2 enrichment and expression levels. RNA-seq experiments were performed in biological triplicates, each yielding between 51 M and 65 M mapped reads. (**a**) Hierarchical clustering of WT and KO expression values Log[1+FPKM] using Euclidean distance metric and mean linkage function. (**b**) Aligned MeCP2-enrichment profile (color) around TSSs (vertical black dashed line), ordered by expression value (curved gray line). Only transcripts with expression exceeding 0.1 FPKM are shown. The bottom plot shows the median MeCP2 enrichment profile in genes organized by expression quartile. (**c**) Distribution of WT expression levels discretized using equidistant thresholds (colors). (**d**) Distributions of MeCP2 enrichments in the 5' end of genes (defined to cover 500 bps downstream of the TSS) with expression levels thresholded as indicated in **c**. Darker shades indicate the central two quartiles. (**e**) Same as **d** but showing MeCP2 enrichment in promoters (defined to cover 100 bps upstream of TSS). (**f**) Volcano-plot showing fold change KO/WT versus significance. Green dots are significantly differentially expressed transcripts (Benjamini p<0.05). (**g**) MeCP2 enrichment versus expression change. The top plot shows the distribution of expression fold changes between KO and WT. The genes are binned using equidistant thresholds (colors); the bottom vertical plots show the distribution of the MeCP2 enrichment 500 bp downstream of corresponding TSSs, with the darker shades indicating the middle two quartiles. (**h**) Gene ontology terms with significantly down-regulated expression in the KO. Bars indicate the mean fold change of the annotated genes, and numbers indicate the Benjamini-Hochberg FDR. Only terms with q<0.1% are shown.

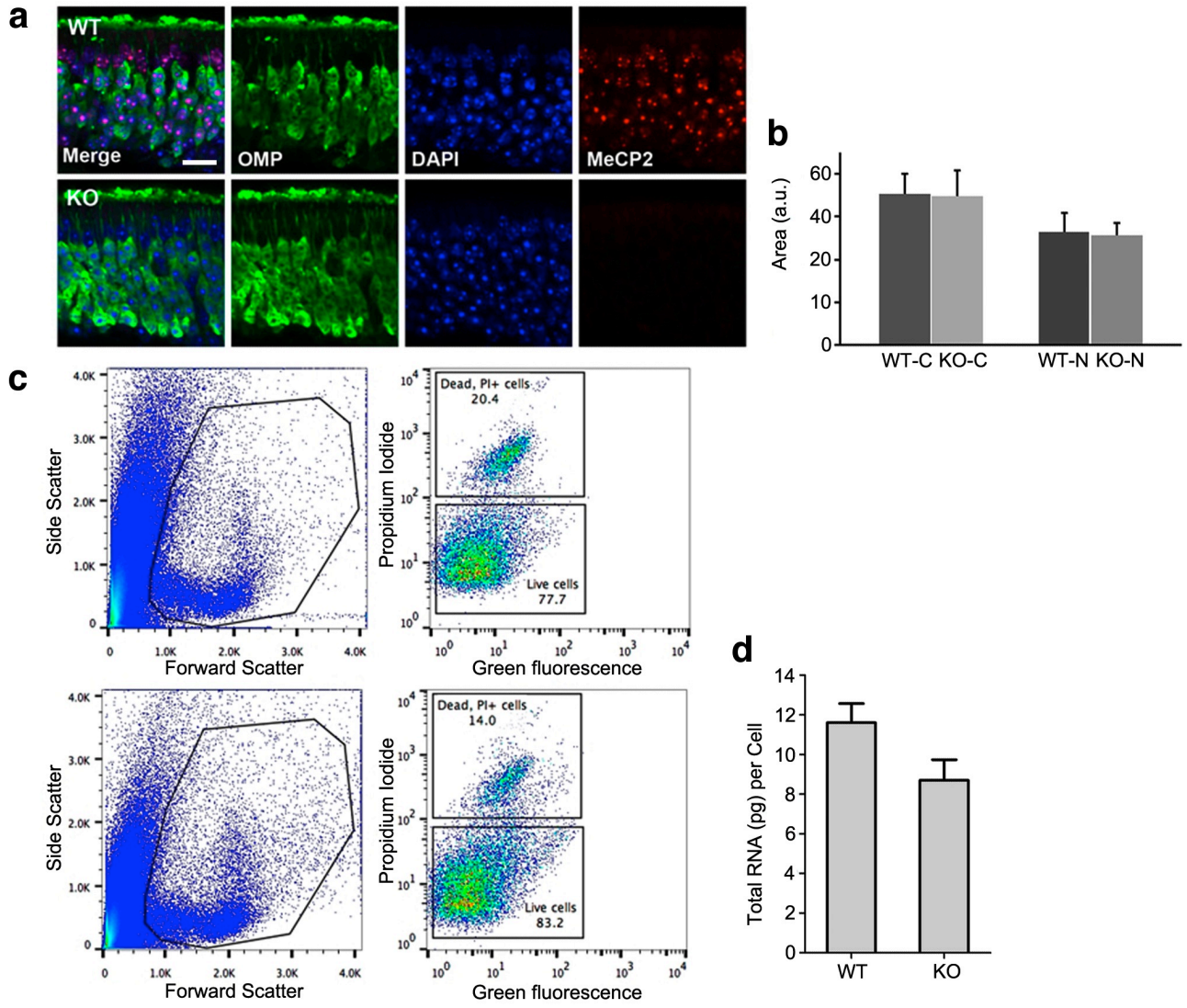

SUPPLEMENTARY FIGURE 10: Measurements of changes in total RNA and cell size between wild-type (WT) and *Mecp2* knockout (KO) olfactory epithelia (OE). (**a**) To compare cell body and nucleus size of olfactory sensory neurons in WT and KO, OE were immunostained with antibodies against olfactory marker protein (OMP, 1:1000, green), MeCP2 (1:1000, red) and counterstained with DAPI for nuclei (blue). MeCP2 signal is absent in the KO as expected. Scale bar represents 20 μm. (**b**) Soma and nucleus sizes were measured in the OE and compared between WT and KO. No difference between cell body (WT-C, n=32; KO-C, n=34, $p > 0.75$) and nuclei (WT-N, n=34; KO-N, n=34, $p > 0.30$). (**c**) To measure changes in total RNA in the OE, olfactory neuroepithelia were dissociated and viable cells are sorted through FACS. Viability of OE cells was indicated as propidium iodide negative and collected and counted. (**d**) Total RNA from the same numbers of viable OE cells from WT (n=2) and KO (n=3) were extracted and measured. Decreased total RNA level was observed in KO when compared to that of the WT (11.6 ± 0.97 pg/cell versus 8.75 ± 1.03 pg/cell). Error bars in **b** and **d** indicate standard deviation.

SUPPLEMENTARY TABLE 1. Realtime PCR primer information for ChIP-seq validation in the BDNF region.

BDNF-1F	AGAATATCAATGCTGGGACTGC
BDNF-1R	TCAGCGTACAGTGTGCTTTCTT
BDNF-2F	GCATATAAAGTTTGCGTGTCCA
BDNF-2R	CCATCCTGAAAAACGTAGAAGG
BDNF-3F	TCTGCTATGCTTTCTCTAGTTCCA
BDNF-3R	TTGCAGAATGGAAGAGAAGTCA
BDNF-4F	CTGACAACCGTCTTGTATTCCA
BDNF-4R	TAACCCACTCTTACCCTCTCCA
BDNF-5F	CAGGTATTCTTTTCCTCGCTGT
BDNF-5R	CGCTCCAAAATCTGACTCTCTC
BDNF-6F	GGTGTGTGTGCGTGTACAGTAG
BDNF-6R	TCCCTCCATCCTCTTGTTCTAA
BDNF-7F	CAATGAAAACATGCTCCAAGAA
BDNF-7R	GCTGTTATGGGGTTATCCTGTC
BDNF-8F	AGAGGTTCAGACAACCAGATCC
BDNF-8R	AAAGTGCCAAATACCTTGGTTG
BDNF-9F	GGAGCACATACTGATCTTGCAG
BDNF-9R	TGTGCAGGTATCTCTGGAACTG
BDNF-10F	GAAATTGATGGGGTGATGATTT
BDNF-10R	GGTTATGCAGCTCTCTTGACCT
BDNF-11F	GCACCACAATTACTTCATGCTT
BDNF-11R	ACTGGGTTTCAGGACATTGAGT
BDNF-12F	GTCCAAAGACCACTCTCTGCTC
BDNF-12R	GCCAAGCCTGTCATTATCTAGG
BDNF-13F	GTGGACTCCCACCCACTTT
BDNF-13R	TCCATTTGATCTAGGCAGAGG
BDNF-14F	GGTGGGTTTCTTTTCTTTCTCTT
BDNF-14R	CCGGATAGCATTACACCAAGTT
BDNF-15F	GAAGCGTGACAACAATGTGACT
BDNF-15R	CACAACTTCTCAGTCCCCTAGC
BDNF-16F	TACGGGTTTGATTCCTCTAAGC
BDNF-16R	CGCCTGACTAAGCCTATTGTGT

SUPPLEMENTARY TABLE 2. Realtime PCR primer and amplicon information for ChIP-seq validation of GC%-associated MeCP2 binding.

Name	Sequence	Amplicon Locus (mm9)
HighGC1-F	CAGCTAACACAGAGGCCACA	chr1:132,950,969-132,951,062
HighGC1-R	GCTACAGGGACTCCTGCTTG	
HighGC2-F	AAGTCTCAGGGTCTCCCCATACA	chr2:163,190,044-163,190,129
HighGC2-R	CATGGAAGGGTCCAGATGCCAG	
HighGC3-F	AGAGTGGGTCAGAGCAGACA	chr2:167,569,660-167,569,742
HighGC3-R	GGCCTCCCTGTGACTCTTTC	
HighGC4-F	GTGCCCTGTTTGTGAGGGTA	chr2:24,272,044-24,272,202
HighGC4-R	CTCTCCCCTCTCAGAGACCC	
HighGC5-F	AGGGAACTGCAGACAATGGG	chr3:87,796,637-87,796,726
HighGC5-R	TCACATCTCACTGGCCACAC	
HighGC6-F	GGCTGTTCCCCCACTAACTC	chr11:117,268,130-117,268,242
HighGC6-R	CAGACAGGGACAGGATGCAG	
HighGC7-F	CCCCAAATAGCAAGGCAAGC	chr11:5,771,081-5,771,208
HighGC7-R	CAGCCCTGCCCTTAGATTCC	
HighGC8-F	GAGTTCAGTGGGGTGAGAGC	chr11:61,472,968-61,473,058
HighGC8-R	CACAGCATACACAGCCCCTA	
HighGC9-F	GAATGGTGGTCTGTGGGAGG	chr19:4,152,836-4,152,970
HighGC9-R	CCATGGCTGGCAGACTGTAA	
LowGC1-F	ATCTGATGATGCGATGGTTG	chr1:57,031,228-57,031,316
LowGC1-R	AACGCAAATGACGATTTTCC	
LowGC2-F	ACGGGAGTGACTGCATTTTC	chr10:112,815,661-112,815,749
LowGC2-R	CCAGGGAAGCATATTTGAAAG	
LowGC3-F	AGGGCCTGAAGGTTTTGTCT	chr11:83,667,373-83,667,452
LowGC3-R	GGGGAATTAACAGCGAGATG	
LowGC4-F	CACAACACCAAGCGATAAACA	chr12:58,086,773-58,086,862
LowGC4-R	TTGCAACGTATTGAGAGCAAA	
LowGC5-F	GCGTACAGAGATTGCTGTCGTA	chr13:23,610,487-23,610,586
LowGC5-R	TTGTCCTTATCCGCATGTCA	
LowGC6-F	ACCTCGAGATTCAGCAAGGA	chr13:89,546,278-89,546,362
LowGC6-R	CACGCACAACAGACATTCAA	
LowGC7-F	ATTACAAGCCCGGTCTCCTT	chr14:62,306,729-62,306,824
LowGC7-R	TTGTGGCTTAGCTCATGGTG	
LowGC8-F	TTGCCACACCTACTTCAAACC	chr14:118,988,545-118,988,628
LowGC8-R	TCATCGTGATCCTCAATAGCC	
LowGC9-F	GAACTTCGAGCCCAGCATT	chr16:94,096,053-94,096,136
LowGC9-R	TCCTAATGGAATCGGTGACA	
LowGC10-F	TGGAATTCGCTGTCTAGCAA	chr17:90,563,175-90,563,272
LowGC10-R	CCTTTGACCTTACAGATTTTAACCA	
LowGC11-F	TGGTGCCCCCTTATAATCAA	chr6:12,644,244-12,644,339
LowGC11-R	GCAGATGCGGTATTTCATCC	
LowGC12-F	GCAGATGAAGCTTCCGAAAA	chr5:123,590,435-123,590,520
LowGC12-R	ACCCAATCCATTCTGTCCTT	
LowGC13-F	AGCATGTTTCTTCGAGTCTTG	chr18:26,938,061-26,938,153
LowGC13-R	AGGACAATCATCTGTTCGACAA	

SUPPLEMENTARY TABLE 3. Oligo information for EMSA

Name	Sequence	GC%	CpG#	Locus (mm9)
HighGC oligos				
HighGC1-F	Biotin-TCTCACTGAAGGTGCGCTAGGGAGATGCTGGGTGGGAAACACGCGGCCGG	64	4	chr1:184,379,735-184,379,784
HighGC1-R	Biotin-CCGGCCGCGTGTTTCCCACCCAGCATCTCCCTAGCGCACCTTCAGTGAGA			
HighGC2-F	Biotin-GCTTCCCACTGCTGAGGCCGGTGCCCGCGGAGCTTCTCCCTACGTATTTA	62	4	chr10:84,595,865-84,595,914
HighGC2-R	Biotin-TAAATACGTAGGGAGAAGCTCCGCGGGCACCGGCCTCAGCAGTGGGAAGC			
HighGC3-F	Biotin-GAGATCCAGGCGGCCCAAGAGCAGCAGACACCGGAGGCCTGCATGCGCCA	68	3	chr11:68,343,455-68,343,504
HighGC3-R	Biotin-TGGCGCATGCAGGCCTCCGGTGTCTGCTGCTCTTGGGCCGCCTGGATCTC			
HighGC4-F	Biotin-TGACTGGAGCCACGCCTCCGGAAGCAGGAATCACATGCCGCGGTAGTTGC	62	4	chr12:25,544,357-25,544,406
HighGC4-R	Biotin-GCAACTACCGCGGCATGTGATTCCTGCTTCCGGAGGCGTGGCTCCAGTCA			
HighGC5-F	Biotin-ACCACCCTCGAGGATGGCTTGGGGTCGGGTGGGAAAGTGAGCCTGGCGTG	66	3	chr13:55,093,651-55,093,700
HighGC5-R	Biotin-CACGCCAGGCTCACTTTCCCACCCGACCCCAAGCCATCCTCGAGGGTGGT			
HighGC6-F	Biotin-CAGCAGCCACAACAACGAGCCCAGAAGGAGCGGCCTCCTCCTCGGCGGGA	68	4	chr14:56,331,426-56,331,475
HighGC6-R	Biotin-TCCCGCCGAGGAGGAGGCCGCTCCTTCTGGGCTCGTTGTTGTGGCTGCTG			
HighGC7-F	Biotin-CTGCACCGCACCTCACAAGTACGCTCGTTCGTCCTCTCCCTCATGCCCAC	62	4	chr15:25,392,536-25,392,585
HighGC7-R	Biotin-GTGGGCATGAGGGAGAGGACGAACGAGCGTACTTGTGAGGTGCGGTGCAG			
HighGC8-F	Biotin-CACTCTTCGGTAGCCTGTTCCTGTGGCGGGAGCTGCTGGAGGTACCGCTG	64	3	chr15:76,165,056-76,165,105
HighGC8-R	Biotin-CAGCGGTACCTCCAGCAGCTCCCGCCACAGGAACAGGCTACCGAAGAGTG			
Methylated HighGC Oligos				
mHighGC1-F	Biotin-TCTCACTGAAGGTG^{m}**C**GCTAGGGAGATGCTGGGTGGGAAACACGCGGCCGG	64	4	chr1:184,379,735-184,379,784
mHighGC1-R	Biotin-CCGGCCGCGTGTTTCCCACCCAGCATCTCCCTAG^{m}**C**GCACCTTCAGTGAGA			
mHighGC2-F	Biotin-GCTTCCCACTGCTGAGGCCGGTGCC^{m}**C**GCGGAGCTTCTCCCTACGTATTTA	62	4	chr10:84,595,865-84,595,914
mHighGC2-R	Biotin-TAAATACGTAGGGAGAAGCTCCG^{m}**C**GGGCACCGGCCTCAGCAGTGGGAAGC			
mHighGC3-F	Biotin-GAGATCCAGGCGGCCCAAGAGCAGCAGACAC^{m}**C**GGAGGCCTGCATGCGCCA	68	3	chr11:68,343,455-68,343,504
mHighGC3-R	Biotin-TGGCGCATGCAGGCCTC^{m}**C**GGTGTCTGCTGCTCTTGGGCCGCCTGGATCTC			
mHighGC4-F	Biotin-TGACTGGAGCCACGCCTC^{m}**C**GGAAGCAGGAATCACATGCCGCGGTAGTTGC	62	4	chr12:25,544,357-25,544,406
mHighGC4-R	Biotin-GCAACTACCGCGGCATGTGATTCCTGCTTC^{m}**C**GGAGGCGTGGCTCCAGTCA			
mHighGC5-F	Biotin-ACCACCCTCGAGGATGGCTTGGGGT^{m}**C**GGGTGGGAAAGTGAGCCTGGCGTG	66	3	chr13:55,093,651-55,093,700
mHighGC5-R	Biotin-CACGCCAGGCTCACTTTCCCACC^{m}**C**GACCCCAAGCCATCCTCGAGGGTGGT			
mHighGC6-F	Biotin-CAGCAGCCACAACAA^{m}**C**GAGCCCAGAAGGAGCGGCCTCCTCCTCGGCGGGA	68	4	chr14:56,331,426-56,331,475
mHighGC6-R	Biotin-TCCCGCCGAGGAGGAGGCCGCTCCTTCTGGGCT^{m}**C**GTTGTTGTGGCTGCTG			
mHighGC7-F	Biotin-CTGCACCGCACCTCACAAGTA^{m}**C**GCTCGTTCGTCCTCTCCCTCATGCCCAC	62	4	chr15:25,392,536-25,392,585
mHighGC7-R	Biotin-GTGGGCATGAGGGAGAGGACGAACGAG^{m}**C**GTACTTGTGAGGTGCGGTGCAG			
mHighGC8-F	Biotin-CACTCTTCGGTAGCCTGTTCCTGTGG^{m}**C**CGGGAGCTGCTGGAGGTACCGCTG	64	3	chr15:76,165,056-76,165,105
mHighGC8-R	Biotin-CAGCGGTACCTCCAGCAGCTCC^{m}**C**GCCACAGGAACAGGCTACCGAAGAGTG			
LowGC				
LowGC1-F	Biotin-ATTATTTCATTTTTTTCTATACGCCGTTAGTAATTTTCGTAGAAAGAACG	28	3	chr4:53,726,428-53,726,477
LowGC1-R	Biotin-CGTTCTTTCTACGAAAATTACTAACGGCGTATAGAAAAAAATGAAATAAT			
LowGC2-F	Biotin-TGAAGTAGACTTAGTAAGTTGAGTATCACGTTTCGTTTCGTTTTTATTTT	30	3	chr16:40,571,836-40,571,885

LowGC2-R	Biotin-AAAATAAAAACGAAACGAAACGTGATACTCAACTTACTAAGTCTACTTCA			
LowGC3-F	Biotin-ATAACATCTGTATATATCGATGCGCTTCGGTATCATGTACATGAATATTC	34	3	chr19:49,142,886-49,142,935
LowGC3-R	Biotin-GAATATTCATGTACATGATACCGAAG CGCATCGATATATACAGATGTTAT			
LowGC4-F	Biotin-TATAGTAACAAAATAACGATGGCGTGTCGTATCAGAGGAGAAATAAATCT	34	3	chr16:75,585,018-75,585,067
LowGC4-R	Biotin-AGATTTATTTCTCCTCTGATACGACACGCCATCGTTATTTTGTTACTATA			
LowGC5-F	Biotin-AGTAGGAGGATGAATACGATTTATAAATATCGCGTATGAAATTCTCAAAG	32	3	chr3:25,282,230-25,282,279
LowGC5-R	Biotin-CTTTGAGAATTTCATACGCGATATTTATAAATCGTATTCATCCTCCTACT			
LowGC6-F	Biotin-ACATTTATTTATTTCTTCGATATAAAGTTTATTAGAACCGCCGCTATGTT	28	3	chr4:110,122,946-110,122,995
LowGC6-R	Biotin-AACATAGCGGCGGTTCTAATAAACTTTATATCGAAGAAATAAATAAATGT			

Methylated LowGC Oligos				
mLowGC1-F	Biotin-ATTATTTCATTTTTTTCTATA^{m}**C**GCCGTTAGTAATTTTCGTAGAAAGAACG	28	3	chr4:53,726,428-53,726,477
mLowGC1-R	Biotin-CGTTCTTTCTACGAAAATTACTAACGG^{m}**C**GTATAGAAAAAAATGAAATAAT			
mLowGC2-F	Biotin-TGAAGTAGACTTAGTAAGTTGAGTATCA^{m}**C**GTTTCGTTTCGTTTTTATTTT	30	3	chr16:40,571,836-40,571,885
mLowGC2-R	Biotin-AAAATAAAAACGAAACGAAA^{m}**C**GTGATACTCAACTTACTAAGTCTACTTCA			
mLowGC3-F	Biotin-ATAACATCTGTATATATCGATG^{m}**C**GCTTCGGTATCATGTACATGAATATTC	34	3	chr19:49,142,886-49,142,935
mLowGC3-R	Biotin-GAATATTCATGTACATGATACCGAAG^{m}**C**GCATCGATATATACAGATGTTAT			
mLowGC4-F	Biotin-TATAGTAACAAAATAACGATGG^{m}**C**GTGTCGTATCAGAGGAGAAATAAATCT	34	3	chr16:75,585,018-75,585,067
mLowGC4-R	Biotin-AGATTTATTTCTCCTCTGATACGACA^{m}**C**GCCATCGTTATTTTGTTACTATA			
mLowGC5-F	Biotin-AGTAGGAGGATGAATA^{m}**C**GATTTATAAATATCGCGTATGAAATTCTCAAAG	32	3	chr3:25,282,230-25,282,279
mLowGC5-R	Biotin-CTTTGAGAATTTCATACGCGATATTTATAAAT^{m}**C**GTATTCATCCTCCTACT			
mLowGC6-F	Biotin-ACATTTATTTATTTCTT^{m}**C**GATATAAAGTTTATTAGAACCGCCGCTATGTT	28	3	chr4:110,122,946-110,122,995
mLowGC6-R	Biotin-AACATAGCGGCGGTTCTAATAAACTTTATAT^{m}**C**GAAGAAATAAATAAATGT			

SUPPLEMENTARY METHODS

Electrophoretic Mobility Shift Assay (EMSA)

Production of recombinant *Mecp2* isoforms 1 and 2 was performed in E. coli by cloning the appropriate cDNAs from expression plasmids (OriGene # MR207745 and #MR226839) into pT7-7 using the restriction enzymes Nde I and Eco RI. pT7-Mecp2 plasmids were sequence validated and transformed into BL21 star cells for protein expression. Following IPTG induction, the soluble fraction of the bacterial lysate was purified via desalting (Hi Prep 26/10 desalting column) followed by ion exchange chromatography on Source Q using an AKTA FPLC (GE Healthcare, Piscataway, NJ). Buffers used are 10 mM Tris pH 7.5, 1 mM EDTA, 10% glycerol, with and without 1 M NaCl. Column fractions were screened by SDS-PAGE, the peak fraction identified, and further validated by western blotting (Supplementary figure 10a). Activity of MeCP2 was examined and quantified by EMSA using methylated double stranded oligos containing methylated CpGs (see Supplementary Table 3). After determining activity, MeCP2 (isoform2) was tested for binding activity against 6 low GC oligos (50 bp in length with 28-34% GC) and 8 high GC oligos (50 bp in length with 62-70% GC). All oligo sequences were selected from the mm9 mouse genome (see Supplementary Table 3). Both forward and reverse oligos were modified with 5'biotin. After complementary annealing, double stranded oligos were used for EMSA. Corresponding methylated oligos, each containing one symmetrically methylated CpG, were also evaluated.

An equal amount of MeCP2 was used in all binding reactions. The binding condition was: 10 mM Tris, 75 mM KCl, 1 mM DTT, 1% glycerol, 20 fmol of biotinylated oligos with 50 ng μl^{-1} of poly dA:dT as competitor (Invivogen, Cat#NC0380747) in 20 μl reaction. After 30 min of binding, DNA/MeCP2 complexes were electrophoresed on 6% polyacrylamide TBE gel. Hybond-N+ nylon was used to immobilize biotinylated oligos. Detection of biotinylated oligos was done using LightShift Chemiluminescent EMSA kit (Thermo Scientific). Collection of images and quantification of chemiluminescent signals were done using ChemDoc-It2 Imager by UVP.

Cross-correlation Analysis

The auto- and cross-correlation functions for ChIP-seq and MNase-seq data sets were calculated using the strand-specific counts of mapped reads at single base pair resolution. Because most base pairs have no reads

mapped to them, the signal is under-sampled at this resolution and the correlations are thus low. Furthermore, the different data sets differed in sequencing depth, making it difficult to compare the cross- and auto-correlations between sets. To address these problems, we modeled the number of reads mapping to track a at position $i = 1 \ldots L$ as $X_{a,i} \sim \mathrm{Pois}(\lambda_{a,i})$, where the sampling rate $\lambda_{a,i}$ is the signal, the statistical properties of which we would like to know. However, the values $\lambda_{a,i}$ are unknown, and we model them as identical random variables that become independent for large genomic separation. The population correlation of the counts is then proportional to that of the sampling rates:

$$\rho\left(X_{1,i}, X_{2,i+\delta}\right) = \rho\left(\lambda_{1,i}, \lambda_{2,i+\delta}\right) \prod_{a=1,2} \sqrt{\frac{\mathrm{Var}[\lambda_a]}{\mathrm{Var}[\lambda_a] + \mathrm{E}[\lambda_a]}}$$

To understand how varying the sequencing depth changes this correlations, consider the reparametrization $\lambda_{a,i} = \alpha_a \, \Lambda_{a,i}$ where α_a is the mean sequencing depth and $\Lambda_{a,i}$ is normalized sampling rate with $\mathrm{E}[\Lambda_a] = 1$. Then

$$\rho\left(X_{1,i}, X_{2,i+\delta}\right) = \rho\left(\Lambda_{1,i}, \Lambda_{2,i+\delta}\right) \prod_{a=1,2} \sqrt{\frac{\alpha_a \mathrm{Var}[\Lambda_a]}{\alpha_a \mathrm{Var}[\Lambda_a] \; + 1}}.$$

When the sequencing depth is much smaller than one, this formula gives $\rho\left(X_{1,i}, X_{2,i+\delta}\right) \ll \rho\left(\Lambda_{1,i}, \Lambda_{2,i+\delta}\right)$<1, consistent with the low correlations observed at single base pair resolution. While it is necessary to know $\mathrm{Var}[\Lambda_a]$ to calculate $\rho\left(\Lambda_{1,i}, \Lambda_{2,i+\delta}\right)$ from $\rho\left(X_{1,i}, X_{2,i+\delta}\right)$, the correlation of the counts scales like $\sqrt{\alpha_1 \alpha_2}$ for $\alpha_a \ll 1/\mathrm{Var}[\Lambda_a]$, and this scaling is useful for relating correlations observed at different sequencing depths. To see how the sample auto- and cross-correlation change with the sequencing depth, first note that $\overline{X_a} \cong \mathrm{E}[X_{a,i}]$ for $L \gg 1$. Furthermore, the sample cross-covariance is $\sum_j \frac{1}{L-1}\left(X_{1,j} - \overline{X_1}\right)\left(X_{2,j+\delta} - \overline{X_2}\right) \cong \mathrm{Cov}\left[X_{1,i}, X_{2,i+\delta}\right]$ for $L \gg 1$ and similarly for the sample variance. Thus, sample cross-correlation $r(X_1, X_2; \delta)$ also scales like $\sqrt{\alpha_1 \alpha_2}$ for $\alpha_a \ll \frac{1}{Var[\Lambda_a]}$. Because the simple power scaling saturates around $\alpha_a \sim 1/\mathrm{Var}[\Lambda_a]$, we chose to present the normalized cross- and auto-correlations at the common sequencing depth $\alpha_{\mathrm{norm}} = \frac{1}{4}$. Thus, the normalized sample correlation is

$$r_{\mathrm{norm}}(X_1, X_2; \delta, \alpha_{\mathrm{norm}}) = r(X_1, X_2; \delta) \prod_{a=1,2} \sqrt{\frac{\alpha_{\mathrm{norm}}}{\bar{X}_a}}.$$

Note that while the choice of absolute normalization α_{norm} is somewhat arbitrary, this normalization procedure allows for rigorous comparison of signals with different sequencing depth. Also note that the assumption that $X_{a,i}$ is Poisson distributed can be significantly relaxed; if X_a is distributed according to some distribution parameterized such that $\mathrm{E}[X_i] = \mu_i$, then

$$\rho(X_1, X_2) = \rho(\mu_1, \mu_2) \sqrt{\prod_{i=1,2} \frac{\mathrm{Var}[\mu_a]}{\mathrm{Var}[\mu_a] + \mathrm{E}[\mathrm{Var}[X_a|\mu_a]]}}$$

The above procedure thus works if $\mathrm{Var}[X_i|\mu_i] = \mu_i$ when $\mu_i \ll 1$, a condition that is true both for the Bernouli and for the Negative Binomial distributions.

SUPPLEMENTARY REFERENCES

1 Baubec, T., Ivanek, R., Lienert, F. & Schubeler, D. Methylation-dependent and -independent genomic targeting principles of the MBD protein family. *Cell* **153**, 480-492, doi:10.1016/j.cell.2013.03.011 (2013).

2 Gabel, H. W. *et al.* Disruption of DNA-methylation-dependent long gene repression in Rett syndrome. *Nature* (2015).

3 Chen, L. *et al.* MeCP2 binds to non-CG methylated DNA as neurons mature, influencing transcription and the timing of onset for Rett syndrome. *Proceedings of the National Academy of Sciences* **112**, 5509-5514 (2015).

4 Lister, R. *et al.* Global epigenomic reconfiguration during mammalian brain development. *Science (New York, N.Y.)* **341**, 1237905 (2013).

5 Stadler, M. B. *et al.* DNA-binding factors shape the mouse methylome at distal regulatory regions. *Nature* (2011).

6 Skene, P. J. *et al.* Neuronal MeCP2 is expressed at near histone-octamer levels and globally alters the chromatin state. *Molecular cell* **37**, 457-468, doi:10.1016/j.molcel.2010.01.030 (2010).

7 Clowney, E. J. *et al.* High-throughput mapping of the promoters of the mouse olfactory receptor genes reveals a new type of mammalian promoter and provides insight into olfactory receptor gene regulation. *Genome research* **21**, 1249-1259 (2011).